UC Santa Cruz

UC Santa Cruz Previously Published Works

Title

A Comparison between the Photoactivation Kinetics of Human and Bovine Rhodopsins

Permalink

https://escholarship.org/uc/item/5r62c2n0

Journal

Biochemistry, 55(50)

ISSN

0006-2960

Authors

Funatogawa, Chie
Szundi, Istvan
Kliger, David S

Publication Date

2016-12-20

DOI

10.1021/acs.biochem.6b00953

Peer reviewed

eScholarship.org Powered by the California Digital Library
University of California

BIOCHEMISTRY
including biophysical chemistry & molecular biology

Article

pubs.acs.org/biochemistry

A Comparison between the Photoactivation Kinetics of Human and Bovine Rhodopsins

Chie Funatogawa, Istvan Szundi, and David S. Kliger*

Department of Chemistry and Biochemistry, University of California, Santa Cruz, Santa Cruz, California 95064, United States

ABSTRACT: Rhodopsin is a G-protein-coupled receptor important for vertebrate vision under dim light conditions. Many studies of the activation mechanism of bovine rhodopsin have been conducted, but there have been relatively few investigations of the human protein. A recent study of the late photointermediates of bovine rhodopsin studies at 15 °C and pH 7.3, 8.0, and 8.7 revealed a rather complex activation mechanism involving two metarhodopsin I_{480} and metarhodopsin II intermediates. Human rhodopsin was studied under these same conditions using time-resolved optical absorption spectroscopy with measurements from 10 μs to 200 ms after photolysis. The results show that the two proteins follow the same photoactivation mechanism, although their kinetics differ significantly. The comparison of bovine and human rhodopsins shows that the initial Schiff base deprotonation equilibrium is more forward shifted in human rhodopsin, and more of the reaction flows through the metarhodopsin I_{380} intermediate in human rhodopsin than in the bovine protein.

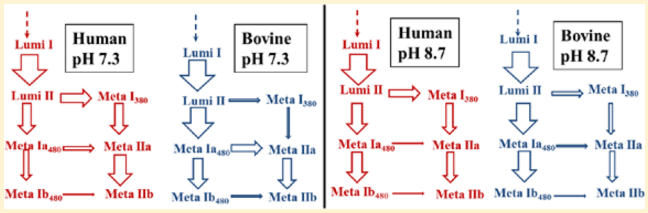

Rhodopsin is a G-protein-coupled receptor (GPCR) found in the rods of photoreceptor cells and is responsible for vision under dim light conditions. It is a heptahelical, transmembrane protein with a retinal chromophore covalently bound to lysine 296 of the protein through a protonated Schiff base linkage. The importance of rhodopsin for vision, and as a model of GPCRs in general, has led to many investigations of the rhodopsin activation mechanism. There are 100 known mutations in various positions in human rhodopsin known to cause several eye diseases such as retinitis pigmentosa.[1,2] Understanding how these mutations affect the activation mechanism of rhodopsin is very important, but to fully understand these effects, knowledge of the activation mechanism of native human rhodopsin is first required. Historically, many studies of rhodopsin activation have been performed on the bovine protein because of the availability[3] of bovine material. This has been viewed as a good model for human rhodopsin because the bovine protein has a sequence that is ~93% homologous to that of human rhodopsin.[4]

Rhodopsin activation is initiated by the photoisomerization of the retinal chromophore from its 11-*cis* to all-*trans* conformation,[5] followed by transformations of a series of intermediates that convert rhodopsin from an inactive to an active state. Once in that state, it interacts with other proteins in the retina. Those interactions result in blocking of sodium channels in rod outer segments, leading to visual transduction. Intermediates in the activation process were first observed in low-temperature trapping experiments that yielded an activation mechanism shown in Scheme 1. Later studies at near-physiological temperatures showed that the activation mechanism was actually more complicated than that revealed at low temperatures, as shown in Scheme 2.

After absorption of light, a red-shifted intermediate, bathorhodopsin (Batho), is formed after the isomerization of the retinal chromophore within picoseconds.[6−8] Batho then forms an equilibrium with a blue-shifted intermediate (BSI) during the relaxation of the chromophore.[9] The Batho/BSI equilibrium decays to form an equilibrium between two lumirhodopsin intermediates, Lumi I and Lumi II; the chromophore continues to relax, and the helices change conformation.[10−13] The Lumi I/Lumi II equilibrium branches to form two metarhodopsin I (Meta I) states. There is a Meta I form absorbing at 480 nm (Meta I_{480}) and a Meta I intermediate absorbing at 380 nm (Meta I_{380}) due to deprotonation of the

Scheme 1. Rhodopsin Activation Mechanism Determined Using Low-Temperature Trapping Methods

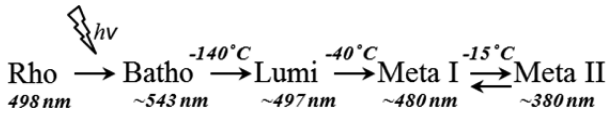

Scheme 2. Rhodopsin Activation Mechanism with the Branched-Square Scheme

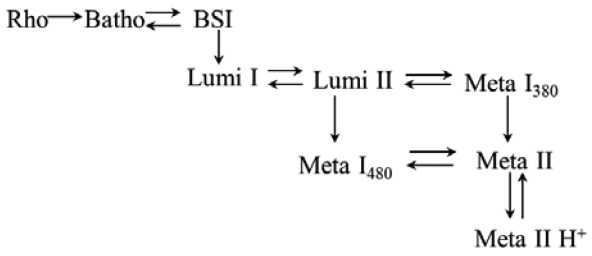

Received: September 19, 2016
Revised: November 17, 2016
Published: November 21, 2016

ACS Publications © 2016 American Chemical Society

DOI: 10.1021/acs.biochem.6b00953
Biochemistry 2016, 55, 7005−7013

Schiff base.[14−17] Finally, a metarhodopsin II (Meta II) intermediate, also with a deprotonated Schiff base, forms. The formation of multiple forms of Meta II involves the movement of helix 6, allowing rhodopsin to bind to transducin. The helix movement also results in a pH-dependent protonation of glutamate 134.[14,18,19]

Previous studies of the human rhodopsin attempted to characterize human rhodopsin intermediates using both temperature trapping and time-resolved spectroscopic measurements to determine the similarities and differences between the activation of human and bovine rhodopsins.[20,21] It was expected that differences in the sequences of human and bovine rhodopsins in the connection from transmembrane 5 and extracellular loop 2 could affect rhodopsin activation and G-protein binding.[21] Other differences between the rhodopsins of the two species involve some differences in the vicinity of the Schiff base, which could affect the electrostatics surrounding the Schiff base, and additional water molecules that could be present in human rhodopsin as a result of serine 297 in the bovine protein being replaced with an alanine in human rhodopsin. This could create more space in the retinal binding pocket for an additional water molecule.[21] The resulting difference in the hydrogen bonding network could cause the shift in the Schiff base deprotonation equilibrium between the observed intermediates of rhodopsin activation.[20,21]

Despite the ∼93% sequence homology, there appears to be significant differences that could affect the activation mechanisms between human and bovine rhodopsins. Studies of the early photointermediates of the two proteins showed that the early intermediates (Batho and BSI) were observed to be spectrally similar in the bovine and human rhodopsins, but the formation of BSI was slower in human rhodopsin.[20] Additionally, the Meta I/Meta II equilibrium was more forward shifted in the human protein.[20,21] At the time of that study, the complex branched-square kinetic scheme (Scheme 2) had not yet been established. Recently, noting some differences between the bovine and human rhodopsin photokinetics led us to study the photoactivation kinetics of bovine rhodopsin at 15 °C and alkaline pHs. This revealed even more complex photokinetics, which led us to introduce a "double-square scheme" (Scheme 3).[22]

Scheme 3. Double-Square Scheme Activation Mechanism

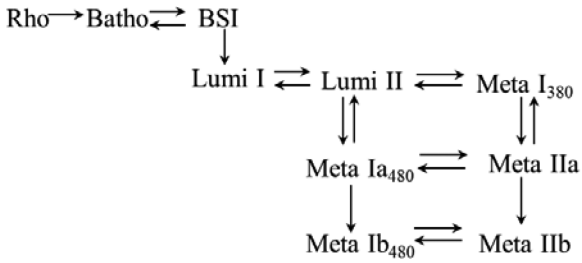

In this study, we investigate the photoactivation of human rhodopsin in membranes on the microsecond to millisecond time scale at 15 °C and pH 7.3, 8.0, and 8.7, to determine whether the photoactivation, like that of bovine rhodopsin, can be described well using the double-square model (Scheme 3) and to discover whether there are differences in the human and bovine photoactivation mechanisms or kinetics. The results indicate the human rhodopsin photoactivation under low temperature and alkaline pH, like that of the bovine protein, is described better by the double-square scheme. Furthermore, the human rhodopsin has a higher net flow through the early Schiff base deprotonation intermediate (Meta I_{380}), and the Schiff base deprotonation is more forward shifted in the last intermediate under these experimental conditions in the human rhodopsin than in the bovine protein. Despite the high degree of sequence homology between the two rhodopsin proteins, there are distinct differences between the photoactivation of human and bovine rhodopsin.

MATERIALS AND METHODS

Hypotonically washed human ROS were isolated, prepared, and sonicated as previously described.[20,23] Washed membranes containing 1 mg of rhodopsin were suspended in 1 mL of 10 mM Tris containing 100 mM NaCl for pH 7.3 and 8.0 experiments and 10 mM BTP with 100 mM NaCl for pH 8.7 experiments. Time-resolved optical absorption difference spectra (post- minus pre-photolysis) were measured from 300 to 700 nm using an apparatus described previously.[9,16] Sample temperatures were maintained at 15 °C. The difference spectra were recorded at delay times from 10 μs to 200 ms following photoexcitation by an ∼7 ns laser pulse from a 477 nm dye laser (80 $\mu J/mm^2$) pumped by the third harmonic of a Nd:YAG laser. Polarization of the probe light was set to 54.7° (magic angle) relative to the excitation pulse polarization to prevent absorbance changes due to the rotational diffusion of rhodopsin.[24]

A data matrix, **A**, containing all of the absorption spectra at delay times from 330 to 650 nm was subjected to singular-value decomposition (SVD) analysis: $\mathbf{A} = \mathbf{U}\cdot\mathbf{S}\cdot\mathbf{V}^{\mathrm{T}}$. Matrix **U** contains the orthogonal basis spectra, matrix **V** contains the orthogonal temporal vectors, and matrix **S** contains the magnitudes of the contributions of the **U** and **V** to the data matrix. The significant **V** vectors were fit to a sum of exponential functions, and the *b*-spectra were calculated as previously described.[9,15] The microscopic rate constants in the proposed kinetic schemes were calculated by fitting kinetic models to the *b*-spectra from the global exponential fit using the proposed intermediate spectra as previously described.[22] All of the calculations were performed using programs written in Matlab (The Mathworks Inc., Natick, MA).

RESULTS

The time-resolved optical absorption difference spectra were recorded after laser excitation at 12 delay times of 5, 10, 30, 50, 100, and 500 μs and 1, 2, 5, 20, 50, and 120 ms for pH 7.3 and 8.7 and 10, 25, 50, 100, and 500 μs and 1, 2, 5, 10, 20, 50, and 120 ms for pH 8.0. The spectra recorded at 15 °C are presented between 330 and 650 nm for pH 7.3, 8.0, and 8.7 in panels a−c of Figure 1, respectively. The data in Figure 1 are normalized to the same protein concentration, and the arrows indicate the direction of absorption change over time in different spectral regions. The collected data sets were subjected to SVD and global exponential fitting analyses. The significant **V** vectors were fit to a sum of exponential functions, assuming the photoinduced reaction follows first-order kinetics. The data sets for the various pHs were best fit using three exponentials with lifetimes of 68 μs, 8.7 ms, and 31 ms for pH 7.3, 62 μs, 7.8 ms, and 25 ms for pH 8.0, and 68 μs, 5.6 ms, and 22 ms for pH 8.7. The error for the lifetimes from multiple experiments is <20%. The corresponding *b*-spectra associated with these lifetimes for pH 7.3, 8.0, and 8.7 are presented in panels a−c of Figure 2,

DOI: 10.1021/acs.biochem.6b00953
Biochemistry 2016, 55, 7005−7013

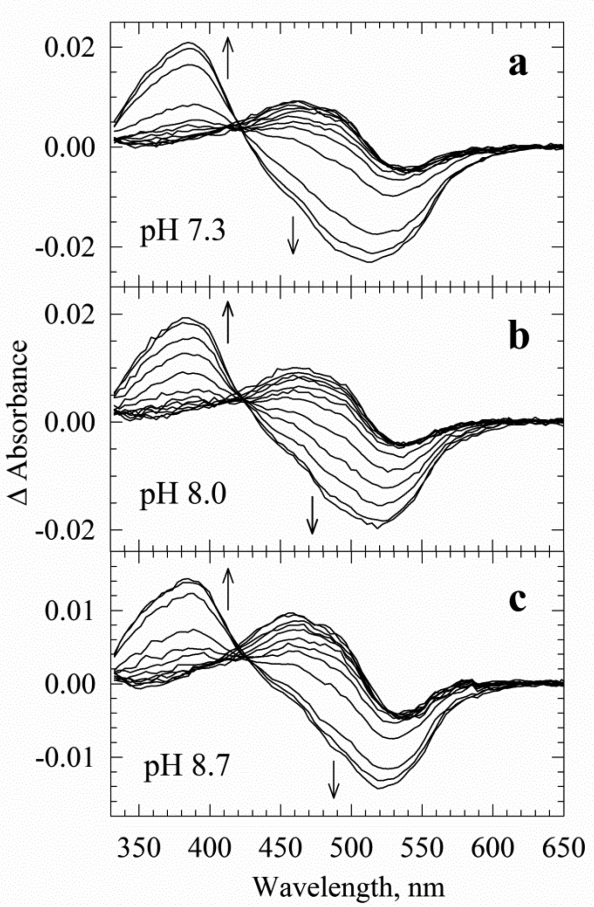

Figure 1. Time-resolved (post- minus pre-photolysis) difference spectra of human rhodopsin membrane suspensions at 15 °C for (a) pH 7.3, (b) pH 8.0, and (c) pH 8.7. The difference spectra were recorded at 12 delay times specified in the text between 10 μs and 120 ms after laser excitation. The arrows indicate the direction of spectral change as the delay time increases.

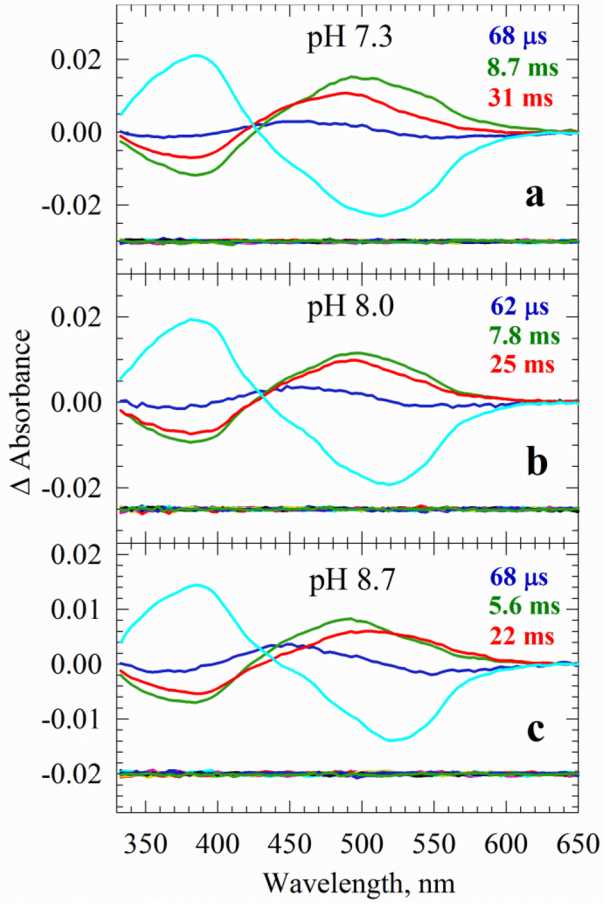

Figure 2. *b* spectra (amplitudes of exponential functions) and apparent lifetimes determined from the global exponential fit for (a) pH 7.3, (b) pH 8.0, and (c) pH 8.7 for human rhodopsin samples. The color of the lifetime presented in each panel matches the color of the corresponding *b*-spectrum: b_1, 62−68 μs (blue); b_2, 5.6−8.7 ms (green); b_3, 22−31 ms (red); b_0 (cyan). b_0 represents the spectrum of the end product for the experimental time scale. The residuals of the three-exponential fit are shown below the *b*-spectra for each pH.

respectively. The final *b*-spectrum, b_0 (colored cyan), represents the spectrum of the end product for the experimental time scale. The residual spectra, which show the difference between the recorded data and the reproduced data based on the exponential fit, are shown below the *b*-spectra in each figure panel. The residual spectra show noise without any significant spectral shapes or features, indicating that a three-exponential fit is adequate for fitting these data sets.

The *b*-spectra, **B**, can be interpreted on the basis of their relationship to the intermediate spectra, **E**, and the eigenvectors, **W**, of the kinetic matrix, **K**.

$$\mathbf{B} = \mathbf{E}\cdot\mathbf{W}$$

The shapes of the *b*-spectra reflect the decay (positive spectral components) and formation (negative spectral components) of intermediates, which could provide essential information about the kinetic scheme.[15]

We start by assuming the simple single-square scheme (Scheme 2) to model the kinetics. The shape of the first *b*-spectra, b_1, colored blue in Figure 2 for each pH, are typical for a Lumi I/Lumi II transition. The second *b*-spectra, b_2, green curves, could be interpreted as transitions from a Lumi I/Lumi II mixture to Meta I_{380}; however, the lifetimes associated with the *b*-spectra are in the millisecond range, whereas the expected lifetime associated with this transition would be much shorter, around 200−500 μs. The third *b*-spectra, b_3, red curves, show positive lobes (decaying intermediates) having red-shifted absorption maxima at higher pHs and negative lobes (intermediates forming) around 380 nm. They can be interpreted as formation of Meta II from mixtures having different compositions depending on the sample pH. The square model (Scheme 2) predicts that this feature is due to Meta II formation from Meta I_{480} alone. These discrepancies from the predictions by the model raise the question of whether the single-square model is valid for human rhodopsin. When tested, using intermediate spectra derived from the sequential intermediates at pH 7.3, as described previously for bovine rhodopsin,[22] the single-square scheme (Scheme 2) failed to reproduce the data sets of the human protein at all pH values. Comparison of the *b*-spectra reproduced by the kinetic fit to the experimental *b*-spectra showed discrepancies similar to those previously described for bovine rhodopsin,[22] and similarly, the misfits by the single-square scheme were most striking at pH 8.7.

We have recently shown[22] that bovine rhodopsin kinetics, under experimental conditions employed in this study, were also poorly described by the square model and required a more complex one, called the double-square model (Scheme 3). The

DOI: 10.1021/acs.biochem.6b00953
Biochemistry 2016, 55, 7005−7013

proposed double-square mechanism was tested by fitting the reaction rate constants to the experimental *b*-spectra and lifetimes as described previously in the kinetic modeling of bovine rhodopsin.[22] Via comparison of our human rhodopsin data with Scheme 3, there are seven intermediate states in the time range explored that would yield six apparent lifetimes and seven *b*-spectra. Global exponential fitting produced three apparent lifetimes and four *b*-spectra. We can assume, as we did for the bovine kinetics, that the transition from Lumi II to Meta I_{380}, occurring presumably with a 250 μs lifetime, shows an amplitude close to zero. This makes the number of experimental apparent lifetimes four and experimental *b*-spectra five. Thus, two lifetimes and *b*-spectra predicted by the model should be regarded as degenerate. Degeneracy of the kinetic matrix caused by specific combinations of reaction rate constants in it, called temporal degeneracy, reduces the number of discrete eigenvalues and eigenvectors, thus reducing the number of lifetimes and *b*-spectra experimentally detected. Because of the presence of isospectral intermediates in the scheme, some of the *b*-spectra may show insignificant amplitude, which is also missed in the exponential fitting. We called this spectral degeneracy. In the case of temporal degeneracy, both the early- and late-millisecond apparent lifetimes were considered degenerate and the corresponding degenerate *b*-spectra were summed up before comparison with the experimental *b*-spectrum was made. In the case of spectral degeneracy, one *b*-spectrum with an unrestricted lifetime, between the early- and late-millisecond experimental lifetimes, was forced to have an insignificant amplitude and only the late-millisecond lifetime was considered degenerate. The submodels representing temporal and spectral degeneracies, which contain different sets of rate constants for the double-square scheme, were found to fit and describe the data set equally well. Therefore, only the fit produced by spectral degeneracy is shown in Figure 3. The *b*-spectra reproduced by the kinetic fit to the double-square scheme (dots) are compared to the experimental *b*-spectra (solid lines) for pH 7.3, 8.0, and 8.7 for human rhodopsin in panels a–c of Figure 3, respectively. The microscopic rate constants in the fitted kinetic matrix for all three pH values are listed in Table 1 for the spectral degeneracy case. As in the case of bovine rhodopsin, the formation of Meta Ia_{480} from Lumi II was found to be practically irreversible at pH 7.3 but reversible at pH 8.0 and 8.7. It is the range, and the relationships between the microscopic rate constants of the different reaction steps in the scheme that have the most physical meaning. This is because multiple solutions, each having its own set of rate constants, can be found even within the spectral degeneracy case by forcing not only one but two of the reproduced *b*-spectra to have amplitudes of nearly zero. However, as discussed in detail in our earlier work,[22] the multiple solutions are reflections of multiple supply and drain pathways leading to and from each intermediate in the scheme. They merely represent different combinations of pathways resulting in the same total inflow and outflow to and from each intermediate in the scheme and thus produce the same buildup and decay rate of intermediate concentrations.

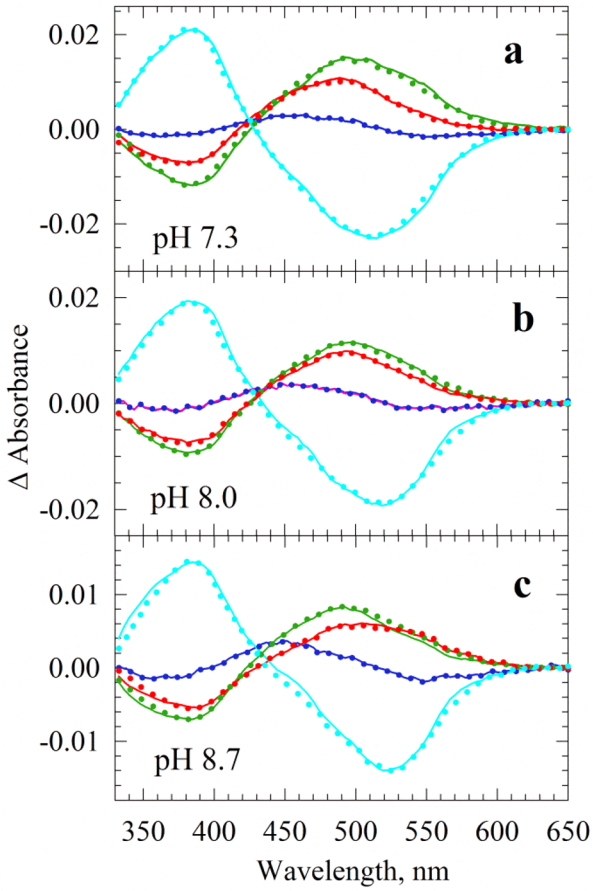

Figure 3. Experimental *b*-spectra (solid lines) presented in Figure 2 with the reproduced *b*-spectra (dotted lines) resulting from the kinetic fit to one of the submodels for the double-square model (Scheme 3) for *b*-spectra b_1 (blue), b_2 (green), b_3 (red), and b_4 (cyan) for (a) pH 7.3, (b) pH 8.0, and (c) pH 8.7. All the various submodels fit equally well.

Table 1. Microscopic Reaction Rate Constants in the Double-Square Submodel with Spectral Degeneracy for Human Rhodopsin

	pH 8.7 $k/-k$	pH 8.0 $k/-k$	pH 7.3 $k/-k$
Lumi I ↔ Lumi II	1.2×10^4/ 3.0×10^3	1.3×10^4/ 3.1×10^3	1.2×10^4/ 2.8×10^3
Lumi II ↔ Meta I_{380}	7.6×10/ 6.4×10^2	7.5×10/ 1.6×10^2	8.2×10/ 3.5×10^2
Lumi II ↔ Meta Ia_{480}	5.7×10/ 2.3×10	6.3×10/ 2.7×10	6.8×10/ 6.8×10^{-3}
Meta I_{380} ↔ Meta IIa	3.0×10^3/ 3.6×10^2	3.3×10^3/ 5.6×10^2	3.6×10^3/ 2.7×10^{-2}
Meta Ia_{480} ↔ Meta IIa	9.0×10^{-1}/2.2	1.3×10/ 1.1×10	2.1×10/6.7
Meta Ia_{480} → Meta Ib_{480}	1.1×10^2/ 1.1×10^{-2}	4.8×10/ 4.8×10^{-3}	1.9×10/ 1.9×10^{-3}
Meta Ib_{480} ↔ Meta IIb	2.0×10/ 2.7×10	2.4×10/ 1.6×10	2.3×10/9.1
Meta IIa → Meta IIb	7.3×10/ 4.1×10^{-3}	7.2×10/ 5.7×10^{-3}	4.5×10/ 5.5×10^{-3}

DISCUSSION

Human rhodopsin follows the complex kinetics described by the double-square model derived for bovine rhodopsin under similar conditions (Scheme 3). A detailed discussion of why this scheme is favored as the one that best fits our experimental results for bovine rhodopsin was presented previously[15,22] and will not be repeated here for our corresponding results for human rhodopsin. The model is characterized by the presence of two Meta I_{480} intermediate states forming in two consecutive steps on the millisecond time scale. These two Meta I_{480} intermediates have protonated Schiff bases and are accompanied by two deprotonated Meta II states. It is presumed that

DOI: 10.1021/acs.biochem.6b00953
Biochemistry 2016, 55, 7005–7013

this complex mechanism is not restricted to the conditions applied in this study but also operational under a wide range of experimental conditions. It may, however, appear that some of the rates and/or intermediates of the complex scheme become undetectable under other conditions, which leads to the appearance of simplifications of the actual mechanism. An example of the latter is the original square model[11,15−17] that has been used to describe the kinetics at more physiological pH values, such as pH 7.3. Under these conditions, the Lumi II-to-Meta Ia_{480} step becomes practically irreversible and two-step Meta I_{480} formation can no longer be detected in UV−vis absorption experiments. It can be recognized only if the Lumi II-to-Meta Ia_{480} step possesses a significant degree of reversibility, as observed at pH 8.7.

Human and bovine rhodopsins both follow the same kinetic pattern, the double-square mechanism. However, there are significant differences between the two proteins with regard to the preferred reaction paths. These differences will be illustrated and interpreted below by comparing the *b*-spectra produced in the global exponential fit, by examining the profiles of the concentration time dependencies of intermediates, and by calculating the net reaction flow through the steps connecting the intermediates in the scheme.

Early Schiff Base Deprotonation Is Enhanced in Human Rhodopsin and Negligible in Bovine Rhodopsin. The apparent lifetimes obtained in the global exponential fitting of the time-dependent absorption data for human and bovine rhodopsin and the corresponding *b*-spectra are compared in Figure 4. The first detected lifetime is around 50−60 μs for human rhodopsin and roughly half of that for bovine rhodopsin. The corresponding *b*-spectra (b_1) reflect the Lumi I-to-Lumi II reversible transition and are very similar at all pHs for both proteins. Figure 4a shows them for human (blue) and bovine (red) forms at pH 8.7.

The second *b*-spectra (b_2) are far more interesting to compare. While the bovine *b*-spectra at all pH values show a Lumi-to-Meta I_{480} transition with negligible formation of the deprotonated Meta form, the *b*-spectra for human rhodopsin report the formation of the deprotonated Meta form to a much greater extent at all pH values. Figure 4b compares the human (blue) and bovine (red) *b*-spectra at pH 8.7. Again, the corresponding lifetimes are longer for human rhodopsin by a factor of roughly 2−3 (5−9 ms for human vs 2−3 ms for bovine). The deprotonated Meta formed on this time scale is Meta IIa rather than Meta I_{380}, which is expected to form on a much faster time scale, 250 μs based on the bovine lifetimes extrapolated to 15 °C, or 500 μs if it also forms slower by a factor of 2. Thus, in human rhodopsin, a large fraction of Lumi II branches in the direction of the deprotonated Meta I_{380} intermediate, which itself decays rapidly into Meta IIa. Bovine rhodopsin branches mainly toward Meta Ia_{480}, as already mentioned, and thus, the reversibility of the Lumi II-to-Meta Ia_{480} step at the different pH values could be estimated from the amplitude of the *b*-spectra. In the case of human rhodopsin, it cannot be done because the *b*-spectra at all pH values contain large negative spectral components at 380 nm due to the formation of the Schiff base deprotonated Meta forms.

The late-millisecond *b*-spectra (b_3) are not drastically different between the two proteins at all three pH values. A comparison is shown in Figure 4c for human (blue) and bovine (red) rhodopsin at pH 8.7. The positive lobe is more red-shifted for human rhodopsin than for bovine rhodopsin, indicating a more back-shifted equilibrium in the Lumi II-to-Meta Ia_{480} transition in human rhodopsin kinetics. Note that the late-millisecond apparent lifetimes are not very different for the two proteins. Thus, the separation between the early- and late-millisecond lifetimes is much smaller for human than for bovine rhodopsin, which affects the accumulation of intermediates, as discussed below.

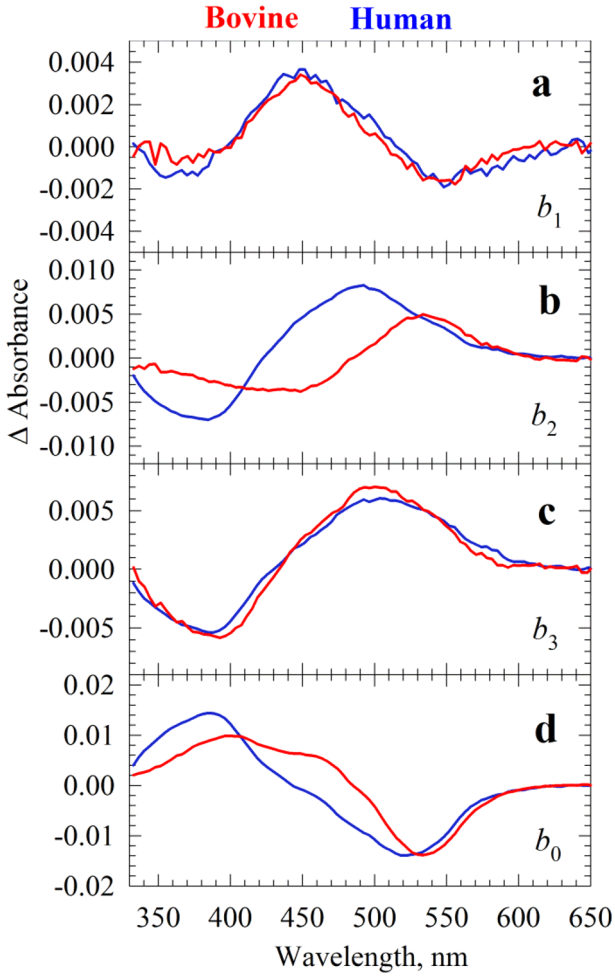

Figure 4. Comparison of the corresponding *b*-spectra, (a) b_1, (b) b_2, (c) b_3, and (d) b_0, of the human (blue) and bovine (red) rhodopsin for pH 8.7. The corresponding lifetimes are 68 and 28 μs for b_1, 5.6 and 2.4 ms for b_2, and 22 and 23 ms for b_3 for human and bovine rhodopsin, respectively.

The enhanced deprotonation of the Schiff base in human rhodopsin, as compared to that in the bovine protein, is also seen in the final *b*-spectra (b_0) at all pH values. A comparison of the pH 8.7 samples is shown in Figure 4d. In the final equilibrium, the fraction of deprotonated Meta IIb is much larger in human (blue) than in bovine (red) rhodopsin.

Time Evolution of Intermediates. The concentration of intermediates that accumulated at any particular time following the initiation of the reaction chain is indispensable information to all experimental techniques, such as infrared and Raman spectroscopy, aimed at obtaining structural information about reaction intermediate forms. While UV−vis spectroscopy is not rich in structural information, it is very effective in deriving reaction mechanisms and determining the microscopic rate constants involved in them. From the latter, the accumulation of intermediates in time can be calculated. Figure 5 shows the time dependence of intermediate concentrations for the

DOI: 10.1021/acs.biochem.6b00953
Biochemistry 2016, 55, 7005−7013

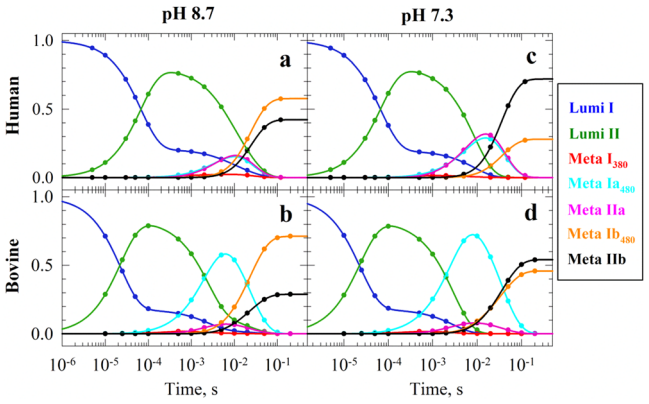

Figure 5. Time evolution of the seven intermediates in the double-square model for samples at pH 8.7 (a and b) and pH 7.3 (c and d) for human (a and c) and bovine (b and d) rhodopsin. The concentration profiles of the Lumi I (blue), Lumi II (green), Meta I_{380} (red), Meta Ia_{480} (cyan), Meta IIa (magenta), Meta Ib_{480} (orange), and Meta IIb (black) spectral forms are displayed between 1 μs and 1 s.

spectral degeneracy case for human and bovine rhodopsin at pH 8.7 (panels a and b, respectively, of Figure 5) and pH 7.3 (panels c and d, respectively, of Figure 5). The data at pH 8.0 yield a case midway between these two pHs and are not shown. Note that the different degeneracy cases involved in the kinetic fitting all produce practically the same time-dependent concentration profiles. At times earlier than 1 ms, Lumi I (blue) and Lumi II (green) are the dominant components and their ratio is fixed in the model fitting. The interesting, and important for other techniques, time window starts slightly below 10 ms. There Meta Ia_{480} (cyan) is the dominant component for bovine rhodopsin at all pH values as seen at pH 8.7 and 7.3 in panels b and d, respectively, of Figure 5. It is well separated from the pre- and postcomponents and thus easily detectable. The accumulation of Meta IIa (magenta) is likely to be insufficient for structural studies under these conditions. Human rhodopsin (panels a and c of Figure 5 for pH 8.7 and 7.3, respectively) shows almost equal levels of accumulation of Meta Ia_{480} (cyan) and Meta IIa (magenta) intermediates. The levels of accumulation, though, are clearly pH-dependent.

At pH 8.7 (Figure 5a), the Meta Ia_{480} and Meta IIa intermediates accumulate to a lesser extent than their precursor Lumi II intermediates do (green), which would make them difficult to detect by structure sensitive techniques. The reversibility of the Lumi II-to-Meta Ia_{480} step is only one of the factors contributing to the low level of Meta Ia_{480} accumulation in human rhodopsin kinetics. The other factor is the insufficient separation between the early- and late-millisecond lifetimes. A ratio of 3−4 separation is observed in the human rhodopsin compared to around 10 for bovine rhodopsin. At pH 7.3 (Figure 5c), the reversibility of the Lumi II-to-Meta Ia_{480} step is no longer a factor and both Meta Ia_{480} (cyan) and Meta IIa (magenta) show a significant level of accumulation; thus, the likelihood of collecting structural information about these intermediate states around a delay of 10 ms is much greater. Comparing panels a and c of Figure 5 and panels b and d of Figure 5 shows that the final intermediate composition of both human and bovine rhodopsin is strongly pH-dependent, showing greater Meta Ib_{480}-to-Meta IIb ratios at higher pH values. Also, comparing the fraction of Meta IIb (black) in the final products for the two proteins confirms that human rhodopsin contains the intermediate species with the deprotonated Schiff base more than bovine rhodopsin. Despite the enhanced early deprotonation of the Schiff base in human rhodopsin, as compared to that of the bovine form, Meta I_{380} (red) does not accumulate to any significant level in the human rhodopsin kinetics, and as in case of bovine rhodopsin, it is practically undetectable at low temperatures.

Dominant Paths of Reaction Flow in Human and Bovine Rhodopsin Kinetics. The level of accumulation of intermediates is important information from the point of view of their structural characterization. However, it tells very little

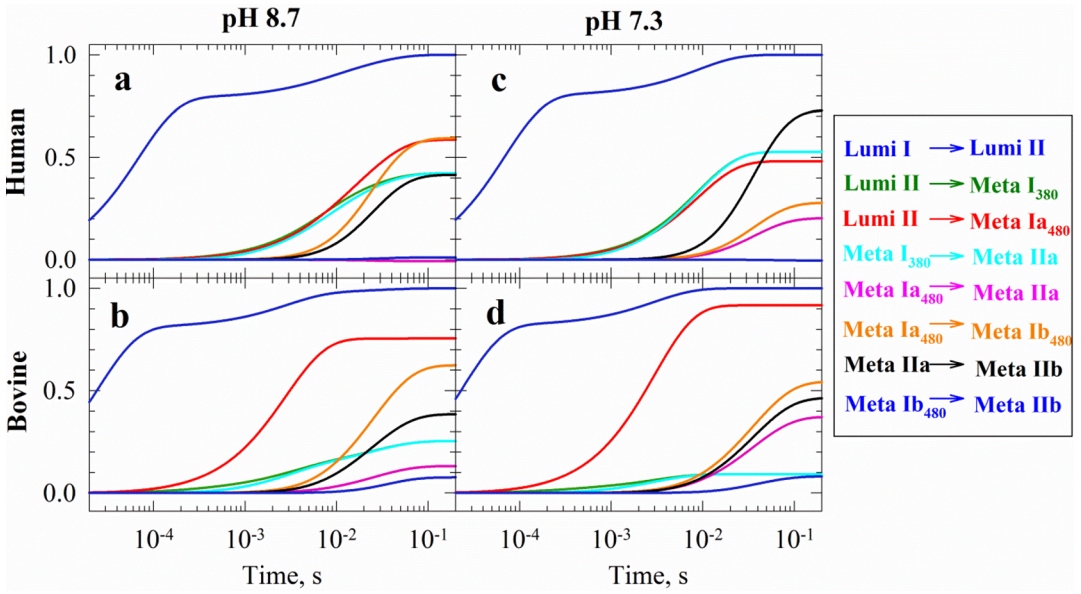

Figure 6. Comparison of the net flow through the eight steps of the double-square model (Scheme 3) for human (a and c) and bovine (b and d) rhodopsin at pH 8.7 (a and b) and pH 7.3 (c and d). The net flow through Lumi I → Lumi II (blue), Lumi II → Meta I_{380} (green), Lumi II → Meta Ia_{480} (red), Meta I_{380} → Meta IIa (cyan), Meta Ia_{480} → Meta IIa (magenta), Meta Ia_{480} → Meta Ib_{480} (orange), Meta IIa → Meta IIb (black), and Meta Ib_{480} → Meta IIb (blue2) spectral forms are displayed between 20 μs and 200 ms.

DOI: 10.1021/acs.biochem.6b00953
Biochemistry 2016, 55, 7005−7013

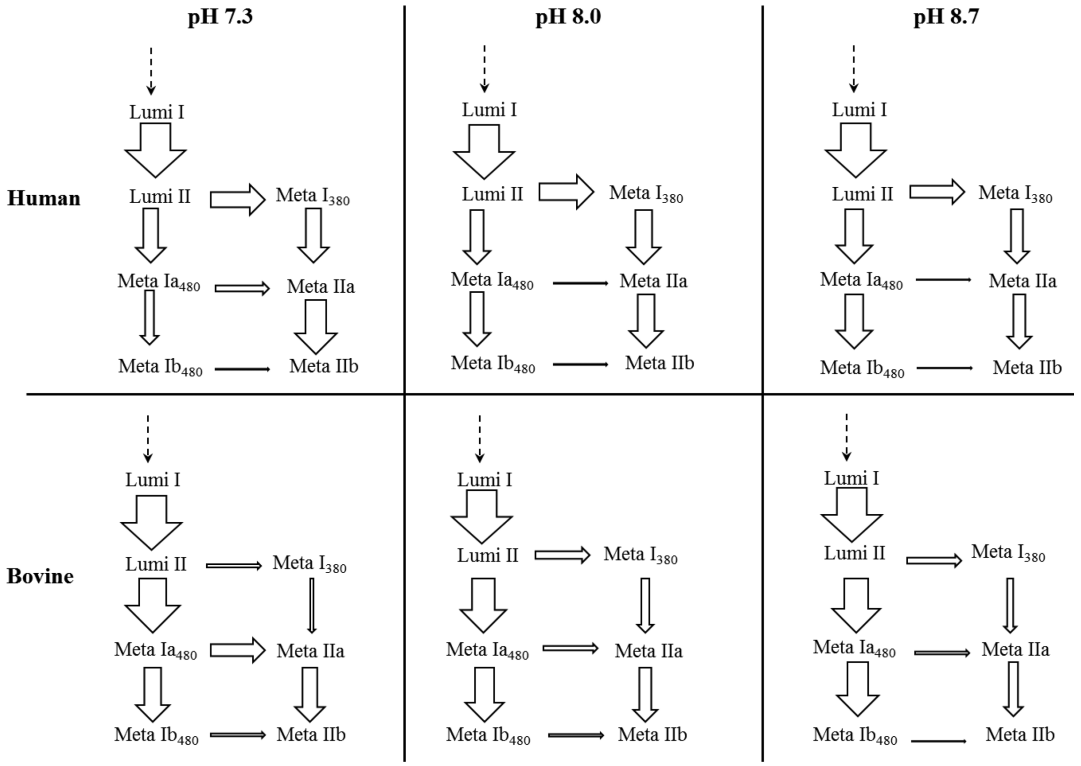

Figure 7. Comparison of the net flow through the eight steps of the late-microsecond to millisecond time scale of the double-square scheme (Scheme 3) for human and bovine rhodopsin at pH 8.7, 8.0, and 7.3 is visualized using arrows. The thickness of the arrows correlates with the amount of flow through those intermediates.

about the reaction path(s) the protein prefers to follow on the energy landscape connecting the first intermediate(s) to the final ones. This is because the level of accumulation of an intermediate is controlled by two opposing factors, the inflow from and the outflow to its neighbors, and thus it is not a reliable measure of the actual reaction flow.

The time-dependent reaction flow rate, $\mathrm{fr}(t)$, through a step connecting two intermediates in the scheme can be calculated on the basis of their time-dependent concentration, $c(t)$, and the forward, k_f, and backward, k_b, rate constants involved in that step. Integration of the flow rate in time gives the time dependence of the net total flow, $\mathrm{tf}(t)$, through that reaction step, as shown below for intermediates A and B:

$$\mathrm{A} \underset{k_b}{\overset{k_f}{\rightleftarrows}} \mathrm{B}$$

$$\mathrm{fr}(t) = k_f c_A(t) - k_b c_B(t)$$

$$\mathrm{tf}(t) = \int \mathrm{fr}(t)\, \mathrm{d}t$$

The net total flow through the eight steps connecting the intermediates in the double-square model is shown in Figure 6, where panels a and b correspond to pH 8.7 and panels c and d to pH 7.3 for human and bovine rhodopsin, respectively. The time scale below 20 μs, which shows only the flow between Lumi I and Lumi II, is cropped to focus on the more complex later steps.

The first interesting observation is the amount of flow through the step connecting Lumi II and Meta I_{380} intermediates (green). Despite the nearly undetectable accumulation of the Meta I_{380} intermediate in both human and bovine rhodopsin kinetics, there is a substantial total flow through this intermediate. In bovine rhodopsin at pH 7.3 (Figure 6d, green), the flow is relatively low but becomes higher at pH 8.7 (Figure 6b, green). The flow is even higher in human rhodopsin, and at pH 7.3 (Figure 6c, green), it matches the flow through the step connecting Lumi II and Meta Ia_{480} (Figure 6c, red). In human rhodopsin, the branching toward the deprotonated Meta forms occurs predominantly at early times, at the Lumi II stage in the scheme, and not later in time at the Meta Ia_{480} or Meta Ib_{480} stage. This is also the tendency for bovine rhodopsin at pH 8.7. For human rhodopsin, deprotonation of the Schiff base at the Meta Ia_{480} stage in the scheme becomes more significant at pH 7.3 (Figure 6c, magenta), and it is the dominant deprotonation path for bovine rhodopsin at this pH (Figure 6d, magenta).

Another interesting observation is the low level of flow through the step connecting the final Meta Ib_{480} and Meta IIb intermediates (Figure 6, the second blue curves, blue2, in all panels) relative to the higher flow through the step between the deprotonated Meta IIa and Meta IIb intermediates (Figure 6, black curves in all panels) in both human and bovine rhodopsin. The time dependence of the total flow for both the human and bovine rhodopsin suggests that most of the Meta IIb seen in the final product is not the result of Meta Ib_{480} undergoing further deprotonation. Instead, it is the consequence of earlier intermediates, Lumi II and Meta Ia_{480}, having the tendency to lose the Schiff base proton at earlier stages to proceed toward the final protein conformation through the deprotonated states. Whether this is a general tendency in rhodopsin kinetics or occurs only at lower temperatures remains an open question.

Through the analysis of the flow described above, it is clear that bovine and human rhodopsin tend to favor different

DOI: 10.1021/acs.biochem.6b00953
Biochemistry 2016, 55, 7005−7013

reaction paths. The discussion of the flow provided above is visualized in the schemes in Figure 7 for human and bovine rhodopsin at pH 7.3, 8.0, and 8.7. The thicknesses of the arrows are proportional to the total net reaction flow through each of the steps in the scheme. It is clear that there is a larger flow through Meta I_{380} in human rhodopsin than in bovine rhodopsin under similar conditions. This indicates that the early Schiff base deprotonation is favored in human rhodopsin. At pH 7.3, Figure 7 shows that most of the Schiff base deprotonation occurs through the Lumi II/Meta I_{380} step in the human rhodopsin, while in bovine rhodopsin, the largest flow leading to Schiff base deprotonation occurs through the Meta Ia_{480}/Meta IIa step.

Human rhodopsin, overall, appears to generate a larger population of early intermediates with a deprotonated Schiff base, as seen by the thicker arrows through Meta I_{380}, Meta IIa, and Meta IIb compared with those of bovine rhodopsin under similar conditions. Furthermore, it is tempting to speculate that Meta IIb is the activated state and, because it is present in higher proportions in the final mixture of intermediates in human versus bovine proteins, that it could influence the relative sensitivity between bovine and human vision. However, because the visual process depends on the enzyme cascade initiated by the activated form of rhodopsin rather than by the yield of the activated state itself, we cannot draw such conclusions from our results. The different paths taken in the two schemes could also lead to a difference in the formation of the inactive metarhodopsin III (Meta III).[25] Previous studies showed that a larger fraction of human rhodopsin converted to Meta III than the fraction in bovine rhodopsin under similar conditions.[26] It is tempting to speculate that Meta III may serve as a storage for all-*trans*-retinal, removing it from the retinoid cycle under bright light and high-bleaching conditions.[25] Recent studies have suggested that excess all-*trans*-retinal may form harmful adducts to rhodopsin and lead to retinal diseases such as age-related macular degeneration[25,27−30] or interfere with the balance of 11-*cis*-retinal, all-*trans*-retinal, and opsin in the regeneration process of rhodopsin. However, further studies are needed to fully understand these factors.

Despite the ∼93% sequence homology between human and bovine rhodopsin, these results clearly indicate a difference in the activation kinetics between the two species. Previous studies comparing human and bovine rhodopsin suggested that the presence of a water molecule near the Schiff base cavity due to the replacement of threonine 297, serine 298, and valine 300 in the bovine protein with serine, alanine, and isoleucine, respectively, may disrupt or change the hydrogen bonding network in the cavity.[21] The change in the hydrogen bonding network could alter the pathway in which Schiff base deprotonation occurs during the activation of rhodopsin. Additionally, the difference in the sequence of the extracellular end of transmembrane 5 connecting to extracellular loop 2 between the two species suggests a change in the movement of the helix, leading to the difference in the activation pathways of human and bovine rhodopsins. Previous studies suggested this transmembrane 5 region could be responsible for some Meta I-like intermediate states.[21]

The lipid environment may also be a factor in the differences observed between human and bovine rhodopsin. These experiments were performed in each protein's native membrane. The human and bovine membrane environments, however, are different. Because the activation of rhodopsin involves a physical movement of the helicies, the lipid environment could affect the activation rate, and also the intermediates favored in the reaction.[31−33] Preliminary results of human and bovine rhodopsin in nanodiscs in our lab indicate that when the rhodopsins are inserted into the nanodiscs with the same lipid environments, the photoactivation kinetics appear to be faster than in the native membrane for both proteins. However, the Schiff base deprotonation equilibria still appear to be different in the same way in the two proteins. This suggests that although the lipid environment does indeed affect the kinetics, the Schiff base deprotonation equilibria remain shifted. Thus, the protein sequence difference between the human and bovine rhodopsin appears to be the dominant factor for this difference.

■ CONCLUSIONS

We have shown that activation of both human and bovine rhodopsins follows the same kinetic scheme represented by the complex double-square model. There are, however, significant differences in the microscopic reaction rate constants and thus in the accumulation of intermediates and the reaction pathways favored by the two proteins. Specifically, human rhodopsin generates more of the intermediates with a deprotonated Schiff base than bovine rhodopsin does under similar conditions. Additionally, at pH 7.3, most of the Schiff base deprotonation occurs at the Lumi II/Meta I_{380} step in human rhodopsin, while in bovine rhodopsin, it occurs mostly at the Meta Ia_{480}/Meta IIa step. The differences probably originate predominantly from the structural differences resulting from the different protein sequences. However, chemical and structural differences in the membranes embedding these two proteins, as well as the different history of the preparations, may also play a role. Preliminary nanodisc studies seem to favor the difference in the protein sequence as the dominant cause of the difference in the activation mechanism.

This study shows the intricacies of the photoactivation mechanism of human rhodopsin and how the equilibrium of Schiff base deprotonation can vary despite the ∼93% sequence homology between the human and bovine rhodopsin. It also suggests that care must be taken in interpreting structural studies of rhodopsin intermediates under different conditions and that under specific conditions dominant intermediates that accumulate in the bovine and human rhodopsins could differ.

■ AUTHOR INFORMATION

Corresponding Author

*E-mail: kliger@ucsc.edu. Phone: (831) 459-2106.

ORCID

Chie Funatogawa: 0000-0002-9355-8155

Funding

This research was supported by National Institutes of Health Grant EY00983 from the National Eye Institute to D.S.K.

Notes

The authors declare no competing financial interest.

■ ACKNOWLEDGMENTS

We thank Erik van Kuijk and the Montana Eye Bank Foundation for providing the donated human retinas. We also thank Jim Lewis for his helpful discussions and advice.

■ ABBREVIATIONS

GPCR, G-protein-coupled receptor; Rho, rhodopsin; ROS, rod outer segments; Batho, bathorhodopsin; BSI, blue-shifted

DOI: 10.1021/acs.biochem.6b00953
Biochemistry 2016, 55, 7005−7013

intermediate; Lumi, lumirhodopsin; Meta, metarhodopsin; BTP, 1,3-bis[tris(hydroxymethyl)methylamino]propane; Tris, tris(hydroxymethyl)aminomethane; SVD, singular-value decomposition.

REFERENCES

(1) Bonilha, V. L., Rayborn, M. E., Bell, B. A., Marino, M. J., Beight, C. D., Pauer, G. J., Traboulsi, E. I., Hollyfield, J. G., and Hagstrom, S. A. (2015) Retinal histopathology in eyes from patients with autosomal dominant retinitis pigmentosa caused by rhodopsin mutations. *Graefe's Arch. Clin. Exp. Ophthalmol. 253*, 2161−2169.

(2) Rakoczy, E. P., Kiel, C., McKeone, R., Stricher, F., and Serrano, L. (2011) Analysis of disease-linked rhodopsin mutations based on structure, function, and protein stability calculations. *J. Mol. Biol. 405*, 584−606.

(3) Wald, G., and Brown, P. K. (1958) Human rhodopsin. *Science 127*, 222−226.

(4) Nathans, J., and Hogness, D. S. (1984) Isolation and nucleotide sequence of the gene encoding human rhodopsin. *Proc. Natl. Acad. Sci. U. S. A. 81*, 4851−4855.

(5) Wald, G. (1968) Molecular basis of visual excitation. *Science 162*, 230−239.

(6) Monger, T. G., Alfano, R. R., and Callender, R. H. (1979) Photochemistry of rhodopsin and isorhodopsin investigated on a picosecond time scale. *Biophys. J. 27*, 105−115.

(7) Peters, K., Applebury, M. L., and Rentzepis, P. M. (1977) Primary photochemical event in vision: proton translocation. *Proc. Natl. Acad. Sci. U. S. A. 74*, 3119−3123.

(8) Schoenlein, R. W., Peteanu, L. A., Mathies, R. A., and Shank, C. V. (1991) The first step in vision: femtosecond isomerization of rhodopsin. *Science 254*, 412−415.

(9) Hug, S. J., Lewis, J. W., Einterz, C. M., Thorgeirsson, T. E., and Kliger, D. S. (1990) Nanosecond photolysis of rhodopsin: evidence for a new, blue-shifted intermediate. *Biochemistry 29*, 1475−1485.

(10) Epps, J., Lewis, J. W., Szundi, I., and Kliger, D. S. (2006) Lumi I → Lumi II: the last detergent independent process in rhodopsin photoexcitationt. *Photochem. Photobiol. 82*, 1436−1441.

(11) Szundi, I., Lewis, J. W., and Kliger, D. S. (2003) Two intermediates appear on the lumirhodopsin time scale after rhodopsin photoexcitation. *Biochemistry 42*, 5091−5098.

(12) Choe, H. W., Kim, Y. J., Park, J. H., Morizumi, T., Pai, E. F., Krauss, N., Hofmann, K. P., Scheerer, P., and Ernst, O. P. (2011) Crystal structure of metarhodopsin II. *Nature 471*, 651−655.

(13) Okada, T., Sugihara, M., Bondar, A. N., Elstner, M., Entel, P., and Buss, V. (2004) The retinal conformation and its environment in rhodopsin in light of a new 2.2 A crystal structure. *J. Mol. Biol. 342*, 571−583.

(14) Jager, S., Szundi, I., Lewis, J. W., Mah, T. L., and Kliger, D. S. (1998) Effects of pH on rhodopsin photointermediates from lumirhodopsin to metarhodopsin II. *Biochemistry 37*, 6998−7005.

(15) Szundi, I., Lewis, J. W., and Kliger, D. S. (1997) Deriving reaction mechanisms from kinetic spectroscopy. Application to late rhodopsin intermediates. *Biophys. J. 73*, 688−702.

(16) Thorgeirsson, T. E., Lewis, J. W., Wallace-Williams, S. E., and Kliger, D. S. (1992) Photolysis of rhodopsin results in deprotonation of its retinal Schiff's base prior to formation of metarhodopsin II. *Photochem. Photobiol. 56*, 1135−1144.

(17) Thorgeirsson, T. E., Lewis, J. W., Wallace-Williams, S. E., and Kliger, D. S. (1993) Effects of temperature on rhodopsin photointermediates from lumirhodopsin to metarhodopsin II. *Biochemistry 32*, 13861−13872.

(18) Altenbach, C., Kusnetzow, A. K., Ernst, O. P., Hofmann, K. P., and Hubbell, W. L. (2008) High-resolution distance mapping in rhodopsin reveals the pattern of helix movement due to activation. *Proc. Natl. Acad. Sci. U. S. A. 105*, 7439−7444.

(19) Mahalingam, M., Martinez-Mayorga, K., Brown, M. F., and Vogel, R. (2008) Two protonation switches control rhodopsin activation in membranes. *Proc. Natl. Acad. Sci. U. S. A. 105*, 17795−17800.

(20) Lewis, J. W., van Kuijk, F. J., Thorgeirsson, T. E., and Kliger, D. S. (1991) Photolysis intermediates of human rhodopsin. *Biochemistry 30*, 11372−11376.

(21) Kazmin, R., Rose, A., Szczepek, M., Elgeti, M., Ritter, E., Piechnick, R., Hofmann, K. P., Scheerer, P., Hildebrand, P. W., and Bartl, F. J. (2015) The Activation Pathway of Human Rhodopsin in Comparison to Bovine Rhodopsin. *J. Biol. Chem. 290*, 20117−20127.

(22) Szundi, I., Funatogawa, C., and Kliger, D. S. (2016) Complexity of Bovine Rhodopsin Activation Revealed at Low Temperature and Alkaline pH. *Biochemistry 55*, 5095−5105.

(23) van Kuijk, F. J., Lewis, J. W., Buck, P., Parker, K. R., and Kliger, D. S. (1991) Spectrophotometric quantitation of rhodopsin in the human retina. *Invest. Ophthalmol. Visual Sci. 32*, 1962−1967.

(24) Lewis, J. W., and Kliger, D. S. (1991) Rotational diffusion effects on absorbance measurements: limitations to the magic-angle approach. *Photochem. Photobiol. 54*, 963−968.

(25) Bartl, F. J., and Vogel, R. (2007) Structural and functional properties of metarhodopsin III: recent spectroscopic studies on deactivation pathways of rhodopsin. *Phys. Chem. Chem. Phys. 9*, 1648−1658.

(26) Lewis, J. W., van Kuijk, F. J., Carruthers, J. A., and Kliger, D. S. (1997) Metarhodopsin III formation and decay kinetics: comparison of bovine and human rhodopsin. *Vision Res. 37*, 1−8.

(27) Fishkin, N., Jang, Y. P., Itagaki, Y., Sparrow, J. R., and Nakanishi, K. (2003) A2-rhodopsin: a new fluorophore isolated from photoreceptor outer segments. *Org. Biomol. Chem. 1*, 1101−1105.

(28) Heck, M., Schadel, S. A., Maretzki, D., Bartl, F. J., Ritter, E., Palczewski, K., and Hofmann, K. P. (2003) Signaling states of rhodopsin. Formation of the storage form, metarhodopsin III, from active metarhodopsin II. *J. Biol. Chem. 278*, 3162−3169.

(29) Rozanowska, M., and Sarna, T. (2005) Light-induced damage to the retina: role of rhodopsin chromophore revisited. *Photochem. Photobiol. 81*, 1305−1330.

(30) Altenbach, C., Yang, K., Farrens, D. L., Farahbakhsh, Z. T., Khorana, H. G., and Hubbell, W. L. (1996) Structural features and light-dependent changes in the cytoplasmic interhelical E-F loop region of rhodopsin: a site-directed spin-labeling study. *Biochemistry 35*, 12470−12478.

(31) Brown, M. F. (1994) Modulation of rhodopsin function by properties of the membrane bilayer. *Chem. Phys. Lipids 73*, 159−180.

(32) Tsukamoto, H., Szundi, I., Lewis, J. W., Farrens, D. L., and Kliger, D. S. (2011) Rhodopsin in nanodiscs has native membrane-like photointermediates. *Biochemistry 50*, 5086−5091.

(33) Wiedmann, T. S., Pates, R. D., Beach, J. M., Salmon, A., and Brown, M. F. (1988) Lipid-protein interactions mediate the photochemical function of rhodopsin. *Biochemistry 27*, 6469−6474.

DOI: 10.1021/acs.biochem.6b00953
Biochemistry 2016, 55, 7005−7013